Shale fracture surface area measured by tracking exchangeable cations

H. Roshan[1,2,*], *M. Sarmadivaleh*[3], *S. Iglauer*[3]

[1]*School of Petroleum Engineering, University of New South Wales, Kensington, Sydney, Australia*

[2]*School of Civil and Environmental Engineering, University of New South Wales Kensington, Sydney, Australia*

*h.roshan@unsw.edu.au

[3]*Department of Petroleum Engineering, Curtin University, Perth, Australia*

Abstract

Hydrocarbon production from oil shale and shale gas is increasingly important for securing the energy supply to society. Such shale reservoirs, however, typically have low permeability, and hydraulic fracturing is required to facilitate economic production. Hydraulic fracturing significantly increases fracture-matrix contact areas (through activating pre-existing fractures as well as creating an artificial fracture network), which is of key importance for efficient production. In this context it is vital to estimate this contact area and associated fracture network structures. Conventional techniques, i.e. micro-seismic mapping and pressure transient analysis, however, only deliver limited information. We thus propose here a new experimental technique, which can measure fracture-matrix contact areas; and the accuracy of contact area measurements can be considerably improved. The proposed technique is based on cation exchange processes and chemical tracer measurements. We verified this technique experimentally with laboratory measurements and demonstrated that fracture-matrix areas can be measured with good precision. It is furthermore possible to gather information about the fracture network structure by conducting transient measurements. We conclude that the proposed technique is feasible, and can be combined with conventional techniques to significantly improve measurement accuracy.

Keywords: Exchangeable cations, Unconventional shale reservoir, Hydraulic fracturing, Fracture network, Flow-back operation, Chemical tracer

1. Introduction

Future energy supply is increasingly relying on shale-gas and oil-shales (Ball and Wietschel, 2009). Typically shale rocks have a low permeability (Civan et al., 2011; Neuzil, 1994; Roshan and Fahad, 2012), and hydraulic fracturing is required to facilitate economic production (Yu et al., 2014). Hydraulic fracturing enhances the hydrocarbon recovery through activating the pre-existing fractures as well as creating an artificial fracture network and therefore increases the fracture-shale matrix contact area where hydrocarbon is accessible (Yost and Overbey, 1989). The structure of the fracture network, especially the contact area per unit volume (fracture density), is one of the key parameters controlling hydrocarbon production from these reservoirs (Arogundade and Sohrabi, 2012; Johri and Zoback, 2013; Mayerhofer et al., 2010). Conventionally, micro-seismic monitoring coupled with pressure transient analysis have been employed to measure fracture-related parameters in tight formations such as shales (Ding et al., 2013; Johri and Zoback, 2013; Nobakht and Clarkson; Reynolds et al., 2012; Rutqvist et al., 2015; Warpinski, 2009; Warpinski et al., 1996). However, micro-seismic monitoring is not always carried out during hydraulic fracturing operations, and if performed, it does not guarantee a successful result due to noise, detector arrangement, small seismic events or large uncertainty stemming from the velocity models (Lockner and Byerlee, 1977; Warpinski, 2009). Furthermore, conventional pressure transient analysis predicts permeability and not fracture surface area; although rate transient analysis can provide the product of surface area and the square root of permeability, but with large uncertainty due to the complexity of flow through fractured shale systems (Nobakht and Clarkson; Reeves and Pekot, 2001). Therefore, knowledge of the structure of the fracture network, and in particular the contact area created by hydraulic fracturing, obtained from these techniques can be severely limited (Ding et al., 2013; Reeves and Pekot, 2001).

In a recent study, Zolfaghari et al (2014) suggested the possibility of characterising the fracture network structure by measuring the salinity of the flowback water versus time; they concluded that if the curve of the salt concentration vs cumulative produced water reaches a plateau, the fracture network is simple (low in density, **Fig. 1a**), whereas a transient salinity variation indicates a complex fracture network (high in density, **Fig. 1b**). While the proposed method is inherently useful, it should be noted that - apart from accessible surface areas - the chemistry of the in-situ pore water, the chemical composition of the shale rocks, and in-situ reservoir conditions all dictate the concentration of salt in the produced water (Musharova, 2012). An increase in aqueous ion concentrations is thus not only a function of the hydraulic fracture network, but also hinges on the cation exchange kinetics (between hydraulic fracturing fluid and clay minerals). Therefore, the amount and type of different dissolved ions should be taken into account when evaluating the fracture network.

We thus hypothesize that a more accurate technique for characterising fractures by chemical tracing is to use cation exchange. The presence of a relatively higher concentration of one major cation (e.g. Na^{+}, Ca^{2+}, K^{+} and Mg^{2+}) than that of shale in the initial composition of the hydraulic fracturing fluid will lead to replacement of the cations on the clay mineral surfaces, and the level of exchange is proportional to the fracture surface area. In practical applications for instance, the concentration of K^{+} is usually relatively high or can be set high in the initial composition of the hydraulic fracturing fluid (Navi et al., 2014). The high concentration of the introduced cation will cause the most prevalent cations in the shale to be exchanged and moved to the bulk solution (Appelo and Postma, 2005; Gray and Darley, 1980). Higher ion concentrations (of the exchanged species) will thus indicate larger fracture surface areas. Similar techniques have been successfully used in soil science to characterise the surface area of clay aggregates (Hepper et al., 2006; Środoń and McCarty, 2008; Yukselen and Kaya, 2006).

In this study, we tested this hypothesis by designing and performing a set of experiments, as described below. The results demonstrate that the proposed technique can indeed measure surface areas of fractures in an aggregate geologic formation with good accuracy.

2. Experimental Methodology

2.1 Shale Material

A calcareous shale core was extracted from 1235 m depth from the Evergreen formation at Surat basin in Queensland, Australia. The Evergreen formation is located beneath a coal formation (Walloon Coal Measures) and above organic-rich shales, the Rewan and Back Creek Groups (ClarkOil&Gas, 2012). The properties of the studied shale were measured and reported previously (Roshan et al., 2015), and therefore the methodologies will only be briefly mentioned here. The mineralogy of the shale sample was measured by XRD as Quartz: 29.1 wt.%; Feldspar: 24.2 wt.%; Kaolinite: 19.8 wt.%; Dolomite: 5.3 wt.%; Illite: 12.8 wt.%; after a 8.80 wt% loss on ignition; and the major elemental oxides in the sample were measured by XRF (in wt%): 62.35 SiO_2, 0.55 TiO_2, 14.16 Al_2O_3, 3.24 Fe_2O_3, 0.27 Mn_3O_4, 0.78 MgO, 5.79 CaO, 1.62 Na_2O, 2.31 K_2O, 0.1 P_2O_5, 8.8 loss on ignition and some traces of Cr, Zr, Sr, Zn, Ni, Ba and Pb. Total Organic Carbon (=1.935wt%) was measured as follows: a sub-sample was crushed to a fine powder in a tungsten carbide ring mill (<100μm grain size) and a portion of the powdered shale sample was treated with HCl to remove inorganic carbonate, then filtered, dried and analysed in duplicate on a LECO CN combustion elemental analyser.

The vitrinite reflectance was determined by measuring the percentage of incident light reflected from a polished sample surface as Ro = 0.52, which indicated that the burial depth was insufficient to lead to thermal maturity, and no hydrocarbon was generated. In addition, the initial pore water saturation was measured as 0.43 by mass balance: the sample was

placed in an oven for 24 hrs at 110 °C (ASTM-D-2216-98, 1999). Finally, the ion displacement method (Andersen et al., 2005) was used to estimate the CEC of the individual major exchangeable cations of the shale sample (i.e. Ca^{2+}, Mg^{2+} and K^{+}). In order to measure the major exchangeable cations, the shale fragments with an average size of 850 μm-1.18 mm were oven-dried for 24 hrs. The sub-crushed aggregates weighing 6.5 g was exposed to 25 ml of 1 M NaCl solution. It was then placed on a ferris wheel for 24 hrs, and then centrifuged at 3000 rpm for 30 min. After the fragment settlement; the supernatant was collected from the shale fragments and filtered through 0.2 μm filter paper. The concentration of major cations was then measured using *ICP-MS* (PerkinElmer quadrapole Nexion instrument) analysis.

2.2 Experimental design and procedure

Two pressure cylinders were designed and built as part of this study. The first cylinder had the internal dimensions of 1 cm (ID) and 5 cm (length). The second cylinder was larger and had 1 cm (ID) and 12 cm (length) dimensions. Each cylinder was equipped with a screw-cap devised with a silicone o-ring for sealing. Brine was injected into the cylinders with a high precision syringe pump (ISCO 500D), thus saturating the fragment packs (see below). The cylinders were housed in a forced-oven to control the shale fragments' temperature and the brines in the pump were heated with a heat jacket installed on the pump syringe to guarantee isothermal conditions (40 °C ±0.5 °C precision). We note that, remarkably, the CEC variation of smectite-clay with temperatures up to 350 °C is insignificant (Emmerich et al., 1999; Gu et al., 2001). This is because the collapse of interlayers of clay minerals occurs at relatively high temperatures. Independent pressure and temperature transducers (Keller LEX) measured the upstream conditions continuously throughout the tests (P&T Digital Gauges, Fig. 2). The schematic of the experimental setup is shown in **Fig. 2**. The experimental procedure consisted of two stages: Stage A and Stage B.

Experiment Stage A:

A sub-core of the shale sample was milled and sieved (Endrock Sieved Machine) to three different fragment sizes: 710 μm-850 μm, 850 μm-1.18 mm and 1.18 mm-1.4 mm. Each mass fraction was oven-dried at 110 °C for 24 hours, and placed in the pressure cylinder (1 cm × 5 cm). Packing was performed by continuously shaking the cylinder with an electrical shaker to make sure that a highly reproducible grain packs are obtained. Subsequently the interfragment porosity was measured by mass balance: the cylinder was weighted before and after adding isopropanol where isopropanol was used to reduce the reaction of clay minerals (Appelo and Postma, 2005). The obtained interfragment porosity was used to calculate the surface area of the fragments per unit volume (SSA) within the cylinder for each mass fraction using the following correlation (Dullien, 1979):

$$SSA = \frac{6(1-\phi)}{dp} \quad (1)$$

where, dp is the average fragment diameter and the fragment shapes are assumed spherical. The isopropanol was then drained out of the cylinder and the cylinder filled with the shale fragments was oven-dried (for 12 hrs at 75 °C), and used for the pressure experiments: the fragment packs were very slowly saturated from the bottom with brine (1M NaCl solution) at an injection rate of 0.2 ml/min for 30 mins until downstream fluid production stabilized. A constant temperature, representing formation temperature, was maintained throughout the tests (40±0.5 ºC). After saturating the pressure cylinder, the downstream valve was closed and the cylinder was pressurised to 2000 psi (13.8 MPa), and after 24 hrs the water was drained by gravity and effluent samples were collected for chemical analysis. The above procedure was carried out for each fragment size tested. Cation concentrations in the effluent volumes were then measured by *ICP-MS*. The alkalinity was also measured by gran titration as 1.4 meq/l on an aliquot of the supernatant to correct for any contribution of Ca^{2+} in the

solution originating from dissolution of calcium carbonate minerals. (Note that for each mole of alkalinity in the supernatant ½ mole of Ca^{2+} should derive from dissolution of carbonate minerals and not the exchanger, (Andersen et al., 2005), assuming no other source of alkalinity). The results presented in the study were thus corrected for contribution of Ca^{2+} in the solution originating from dissolution of calcium carbonate minerals by measured alkalinity.

Experiment Stage B:

The long pressure cylinder (1 cm ×12 cm) was filled with all three mass fractions, a 4 cm layer of the coarse fragments (1.18 mm-1.4 mm) at the bottom, a 4 cm layer of medium sized fragments (850 µm-1.18 mm) in the middle, and a 4 cm layer of finer fragments (710 µm-850 µm) on the top. Again the fragments were packed tightly by continuously shaking the cylinder during packing. The filled cylinder was then saturated as in stage A, at the same temperature and pressure. After 24 hrs, the water was drained out by gravity and 6 effluent samples were collected successively, each had a volume of 0.5 ml (10 drops), for the chemical analysis. Stage B was designed to verify the correlations obtained in stage A. These correlations estimate the surface area between fractures and matrix (via ion mass content measurements which is discussed further below). Eventually, a coarse fragment sample was exposed to deionised (DI) water at standard conditions at different times (4, 24 and 48 hrs) and cation concentrations in the effluent where analysed to investigate the associated reaction kinetics.

3. Experimental Results and Discussion

Interfragment porosities and associated specific surface areas (SSA, surface area per volume, cp. equation 1) decreased with increasing fragment size, **Fig. 3** (Rogers and Head, 1961).

These fragment packs can represent different fracture densities; the finer fragments pack with a high SSA mimics a fracture network with high fracture density, and the coarse fragment pack a low fracture density.

The effect of the fracture aperture is also embedded in the fragments pack models **(Fig. 4)**, e.g. if a fracture's aperture (b) within a block increases to 2b (without any change in block size), the contact area remains unchanged while the volume of the fracture doubles and thus the ion concentration is halved (where ion mass content is constant). We note that the fracture aperture influences the position of the correlation between the ion concentration and SSA, (Figure 4) however the contact area is eventually correlated to the ion mass content and therefore it is independent of fracture volume. Additional information about the fractures' apertures in the system could thus be obtained through analysing the concentration against surface area.

In the first set of tests (stage A), the fragments packs were saturated with 1M NaCl and therefore the major exchangeable cations (Ca^{2+}, K^{+} and Mg^{2+}) were expected to be replaced by Na^{+}. This was indeed the case for Ca^{2+} and K^{+}, for which increased aqueous concentrations were measured after 24 hrs and converted to cation mass content (**Fig. 5).** The data was well-fitted with logarithmic functions, consistent with the trend of the field data presented by Zolfaghari et al (2014), for all cations considered (cp. equation 2-4; $R^2 = 0.999$ for Ca^{2+}, $R^2 = 0.981$ for K^{+}, $R^2 = 0.548$ for Mg^{2+}), however, only the Ca^{2+} and K^{+} aqueous cation mass contents significantly increased with increasing SSA (Fig. 5):

$$MC_{Ca} = 0.2327 \ln(SSA) - 0.5481 \quad (2)$$

$$MC_{K} = 0.1679 \ln(SSA) - 0.5237 \quad (3)$$

$$MC_{Mg} = 0.002 \ln(SSA) + 0.0002 \quad (4)$$

For the layered fragment pack (stage B), Ca^{2+} and K^{+} concentrations also increased with cumulative water production, while the concentration of Mg^{2+} remained almost unchanged (**Fig. 6**). This increase in ion concentration in stage B is correlated to the accessible surface area of the shale fragments: the surface area increased from the bottom to the top part of the cylinder (fragment sizes shrank, cp. section 2) and therefore higher concentrations were measured at higher drainage times (i.e. larger cumulative drained water volumes after a constant dwell time of 24 h). We note that the concentration of exchanged cations depends on the presence of these cations in the exchange sites of the minerals (Rao and Mathew, 1995); the very low concentration of Mg^{2+} in the solution indicates that Mg^{2+} ions are either not available or not significantly accessible, consistent with the low Mg concentrations measured in the shale sample (0.78 wt% MgO, cp. section 2.1). Calcium was much more abundant (5.79 wt% CaO), and significantly higher exchanged concentrations were measured in the aqueous phase, while Potassium showed an intermediate response (with an intermediate concentration in the original shale, 2.31 wt%). We thus conclude that cation concentration in the shale is likely to considerably influence observed aqueous concentrations.

3.1. Cation Exchange Capacity of individual cations as a criterion

In order to assess which cation is best suited for surface area measurements, the cation exchange capacities (*CEC*) of each cation were calculated and reported in **Table 1.** From Table 1, it is seen that Ca^{2+} had a significantly higher CEC than K^{+} and Mg^{2+} (ranking: $Ca^{2+}>K^{+}>Mg^{2+}$), and we thus conclude that Ca^{2+} is the best cation for surface area measurements. This is demonstrated that the individual CEC can be used to evaluate the most suitable major exchangeable cation for measuring the surface areas of shale formations. It is, however, noted that the most suitable exchangeable cation depends on the chemical composition of shale and therefore the CEC test of individual cations should be conducted for

each material. Moreover, it is noteworthy that there is no correlation between shale clay content and SSA, and therefore clay content cannot be used as a criterion (Yukselen and Kaya, 2006). This is due to the fact that higher clay content does not necessarily lead to higher CEC as it also depends on the type of clay minerals present in the sample (Yukselen-Aksoy and Kaya, 2010). In addition, the cation concentration in the shale cannot be used instead of CEC as cation concentration is not always correlated to the individual CEC.

3.2. Estimation of surface area from cation concentrations

Surface areas, in stage B experiment, can be estimated by measuring aqueous cation mass contents (from ion concnetration and the solution volume/produced water), and substituting them into Eqs. 2, 3 or 4. With the sum of the total cation mass content (i.e. the sum of all mass contents measured in all effluents), the total SSA of the system can be determined (**Figure 7** for the layered pack). The measuurments of the cation masss content for each efflunet also gives information about the dynamic variation of the surface area in the tested formations.

Specifically, the total SSA of the layered pack in the long cylinder (stage B) was estimated as 106.5 cm^2/cm^3 (using Eq. 1). The total specific surface areas determined via total cation measurements (Fig. 7) were then compared to this benchmark (**Fig. 8).** It is evident from Figure 8 that the SSA obtained from the Ca^{2+} correlation is predicted quite accurately, while SSA from K^+ and Mg^{2+} over- and underestimate SSA. This is attributed to the fact that the proposed correlation is best fitted to the Ca^{2+} concentration (Fig. 5); which is due to the considerably higher CEC for Ca^{2+} (than for K^+ or Mg^{2+}, Fig. 7): the higher Ca^{2+} CEC results in higher Ca^{2+} mass transfer into the bulk solution from the shale which in turn leads to more accurate measurements.

3.3 Cation exchange reaction kinetics

The coarse fragment pack was also exposed to DI water for specific times (4, 24 and 48 hrs) to measure the cation exchange kinetics. The results are summerised in **Table 2**; while virtually all exchange took place within the first 4h for Ca^{2+}, a minor increase in K^{+} concentration was observed after 48 hrs. The reaction velocity for Mg^{2+} was slow, and significant concentration changes were observed between 4h, 24h and 48h. This behaviour is consistent with literature reported for potassium and sodium exchange into different clay minerals (Sparks and Jardine, 1984).

3.4 Limitations and application of the proposed technique

The proposed technique (of estimation the specific surface area of fractures using CEC measurements) can only be used if the shale contains active clay minerals, where cation exchange can occur. The cations are exchanged between the cations present in the hydraulic fracturing fluid and the clay minerals as well as organic matters. If the shale formation has a very low CEC, the application of the method will be limited. Thus the individual CECs of each major cation should be measured to gain confidence in the applicability of the method and to establish the correct correlations. In addition, the results are not affected by the adsorbed water into shale matrix; however, the unrecovered water within the fracture network of the shale could influence the results. Moreover, if the quantitative estimation of the productive fracture surfaces is required; the specific surface area obtained by the proposed technique can be multiplied with the stimulated volume of the reservoir. The stimulated volume could be estimated via micro-seismic measurements (Mayerhofer et al., 2010; Zimmer, 2011).

4. Conclusions

A novel, easy and cost efficient technique was introduced in this study to measure hydraulic fracture density (surface area between fractures and matrix) in aggregate geologic formations. This method can be combined with conventional techniques such as pressure transient analysis (Ding et al., 2013) and micro-seismic monitoring (Johri and Zoback, 2013; Lockner and Byerlee, 1977) for more accurate estimation of fracture surface area, and it only requires a small amount of (preserved) formation sample, several low-cost experiments to determine the surface areas, and flow back water sampling. Specifically, the specific surface area is measured via aqueous phase cation mass content measurements, which are correlated to the matrix-fracture surface areas. Chemically, a higher concentration of one major exchangeable cation in the fracturing fluid leads to replacement with clay-bound cations. The cation mass content and associated exchange kinetics are thus indicators of the accessible surface area.

The advantage of this technique over a) pressure transient analysis is that no complex mathematical framework is needed, (Dinh et al.) which makes the method more applicable to field settings with higher accuracy, and b) micro-seismic monitoring is that the micro-seismic monitoring is not always carried out during hydraulic fracturing operations, and if conducted, it does not guarantee a successful result due to noise, detector arrangement, small seismic events or large uncertainty stemming from the velocity models (Lockner and Byerlee, 1977; Warpinski, 2009). In conclusion, a combination of the suggested chemical tracer technique with conventional methods could lead to substantially improved fracture density measurements, which is of key relevance in hydraulic fracturing operations and associated production predictions (Arogundade and Sohrabi, 2012).

References

Andersen, M.S., Nyvang, V., Jakobsen, R. and Postma, D., 2005. Geochemical processes and solute transport at the seawater/freshwater interface of a sandy aquifer. Geochimica et Cosmochimica Acta, 69(16): 3979-3994.

Appelo, C.A.J. and Postma, D., 2005. Geochemistry, groundwater and pollution. Taylor&Francis, Amesterdam.

Arogundade, O. and Sohrabi, M., 2012. A Review of Recent Developments and Challenges in Shale Gas Recovery, SPE Saudi Arabia Section Technical Symposium and Exhibition. Society of Petroleum Engineers, Al-Khobar, Saudi Arabia.

ASTM-D-2216-98, 1999. Standard Test Method for Laboratory Determination of Water (Moisture) Content of Soil and Rock by Mass American Society for Testing and Materials, West Conshohocken.

Ball, M. and Wietschel, M., 2009. The future of hydrogen – opportunities and challenges. International Journal of Hydrogen Energy, 34(2): 615-627.

Civan, F., Rai, C. and Sondergeld, C., 2011. Shale-Gas Permeability and Diffusivity Inferred by Improved Formulation of Relevant Retention and Transport Mechanisms. Transport in Porous Media, 86(3): 925-944.

ClarkOil&Gas, 2012. Shale Gas Opportunity in the Surat Basin, Australia. Clark Oil & Gas, Queensland, Australia.

Ding, D.Y., Wang, C. and Wu, Y.-S., 2013. Characterizing Hydraulic Fractures in Shale Gas Reservoirs Using Transient Pressure Tests, SPE Hydraulic Fracturing Technology Conference. Society of Petroleum Engineers, The Woodlands, Texas, USA.

Dinh, V.P., Gouge, B.A. and White, A.J., Estimating Long Term Well Performance in the Montney Shale Gas Reservoir. Society of Petroleum Engineers.

Dullien, F.A.L., 1979. Porous Media Fluid Transport and Pore Structure. Academic Press, New York.

Emmerich, K., Madsen, F.T. and Kahr, G., 1999. Dehydroxylation behavior of heat-treated and stream-treated homoionic Cis-vacant montmorillonites. Clays and Clay Minerals, 47(5): 591-604.

Gray, G.R. and Darley, H.C.H., 1980. Composition and Properties of Oil Well Drilling Fluids. Gulf Publishing Company, Houston.

Gu, B.X., Wang, L.M., Minc, L.D. and Ewing, R.C., 2001. Temperature effects on the radiation stability and ion exchange capacity of smectites. Journal of Nuclear Materials, 297(3): 345-354.

Hepper, E.N., Buschiazzo, D.E., Hevia, G.G., Urioste, A. and Antón, L., 2006. Clay mineralogy, cation exchange capacity and specific surface area of loess soils with different volcanic ash contents. Geoderma, 135: 216-223.

Johri, M. and Zoback, M.D., 2013. The Evolution of Stimulated Reservoir Volume during Hydraulic Stimulation of Shale Gas Formations, Unconventional Resources Technology Conference. Society of Petroleum Engineers, Denver, Colorado, USA.

Lockner, D. and Byerlee, J.D., 1977. Hydrofracture in Weber Sandstone at high confining pressure and differential stress. Journal of Geophysical Research, 82(14): 2018-2026.

Mayerhofer, M.J. et al., 2010. What Is Stimulated Reservoir Volume? SPE Production & Operations, 25(1).

Musharova, D., 2012. The Effect of Physico-Chemical Factors on the Stability and Transport of Clay Particles, Texas A&M University, Texas.

Navi, M., Skelly, C., Taulis, M. and Nasiri, S., 2014. Coal seam gas water: potential hazards and exposure pathways in Queensland. International Journal of Environmental Health Research, 25(2): 162-183.

Neuzil, C.E., 1994. How permeable are clays and shales? Water Resources Research, 30(2): 145-150.

Nobakht, M. and Clarkson, C.R., A New Analytical Method for Analyzing Linear Flow in Tight/Shale Gas Reservoirs: Constant-Flowing-Pressure Boundary Condition.

Rao, S.N. and Mathew, P.K., 1995. Effects of Exchangeable Cations on Hydraulic Conductivity of a Marine Clay. Clays and Clay Minerals, 43(4): 433-437.

Reeves, S. and Pekot, L., 2001. Advanced Reservoir Modeling In Desorption-Controlled Reservoirs, SPE Rocky Mountain Petroleum Technology Conference. Society of Petroleum Engineers, Keystone, Colorado.

Reynolds, M.M. et al., 2012. A Direct Comparison of Hydraulic Fracture Geometry and Well Performance Between Cemented Liner and Openhole Packer Completed Horizontal Wells in a Tight Gas Reservoir, SPE Hydraulic Fracturing Technology Conference. Society of Petroleum Engineers, The Woodlands, Texas, USA.

Rogers, J.J.W. and Head, W.B., 1961. Relationships between porosity, median size, and sorting coefficients of synthetic sands. Journal of Sedimentary Research, 31(3): 467-470.

Roshan, H., Ehsani, S., Marjo, C.E., Andersen, M.S. and Acworth, R.I., 2015. Mechanisms of water adsorption into partially saturated fractured shales: An experimental study. Fuel, 159: 628-637.

Roshan, H. and Fahad, M., 2012. Chemo-poroplastic analysis of a borehole drilled in a naturally fractured chemically active formation. International Journal of Rock Mechanics and Mining Sciences, 52(0): 82-91.

Rutqvist, J., Rinaldi, A.P., Cappa, F. and Moridis, G.J., 2015. Modeling of fault activation and seismicity by injection directly into a fault zone associated with hydraulic fracturing of shale-gas reservoirs. Journal of Petroleum Science and Engineering, 127(0): 377-386.

Sparks, D.L. and Jardine, P.M., 1984. COMPARISON OF KINETIC EQUATIONS TO DESCRIBE POTASSIUM-CALCIUM EXCHANGE IN PURE AND IN MIXED SYSTEMS. Soil Science, 138(2): 115-122.

Środoń, J. and McCarty, D.K., 2008. Surface area and layer charge of smectite from CEC and EGME/H2O-retention Measurements. Clays and Clay Minerals, 56(2): 155-174.

Warpinski, N., 2009. Microseismic Monitoring: Inside and Out. Journal of Petroleum Technology.

Warpinski, N.R. et al., 1996. Microseismic Monitoring of the B-Sand Hydraulic-Fracture Experiment at the DOE/GRI Multisite Project.

Yost, A.B. and Overbey, W.K., Jr., 1989. Production and Stimulation Analysis of Multiple Hydraulic Fracturing of a 2,000-ft Horizontal Well, SPE Gas Technology Symposium. Society of Petroleum Engineers, Dallas, Texas.

Yu, W., Luo, Z., Javadpour, F., Varavei, A. and Sepehrnoori, K., 2014. Sensitivity analysis of hydraulic fracture geometry in shale gas reservoirs. Journal of Petroleum Science and Engineering, 113(0): 1-7.

Yukselen-Aksoy, Y. and Kaya, A., 2010. Method dependency of relationships between specific surface area and soil physicochemical properties. Applied Clay Science, 50(2): 182-190.

Yukselen, Y. and Kaya, A., 2006. Comparison of Methods for Determining Specific Surface Area of Soils. Journal of Geotechnical and Geoenvironmental Engineering, 132(7): 931-936.

Zimmer, U., 2011. Calculating Stimulated Reservoir Volume (SRV) with Consideration of Uncertainties in Microseismic-Event Locations, Canadian Unconventional Resources Conference. Society of Petroleum Engineers, Calgary, Alberta, Canada.

Zolfaghari Sharak, A., Ghanbari, E., Dehghanpour, H. and Bearinger, D., 2014. Fracture Architecture from Flowback Signature: A Model for Salt Concentration Transient, SPE Hydraulic Fracturing Technology Conference. Society of Petroleum Engineers, The Woodlands, Texas, USA.

Table 1. Individual CEC based on cations concentrations measured by ICP-MS analysis using ion displacement with NaCl solution (corrected for calcium dissolution).** value not given due to interference from testing method.

Table 2. Aqueous cation concentrations as a function of time for the coarse fragment pack (1.18 mm-1.4 mm fragment size) exposed to DI water.

Fig. 1. Structure of a simple (a) and complex (b) fracture network.

Fig. 2. Schematic of the experimental setup.

Fig. 3. The specific surface area and interfragment porosity of the fragment packs as a function of fragment size.

Fig. 4, Effect of fracture aperture on the estimation of SSA.

Fig. 5. Aqueous ion mass content after cation exchange versus Specific Surface Area.

Fig. 6. Aqueous phase cation concentrations versus cumulative drained water volume (layered pack).

Fig. 7. Specific surface area estimated from the correlations presented in Eqs. 2 to 4 versus cumulative drained water (the total SSA is the sum of all individual SSAs).

Fig. 8. Relative error between the measured and estimated specific surface area.

Highlights

- Contact area of fractures in shale formations is characterised by chemical tracer
- Major exchangeable cations are tracked to obtain the structure of fracture network in shales
- A set of novel tests are proposed to characterise the fracture network structure
- The proposed technique is simple, cost efficient and precise

Figure1

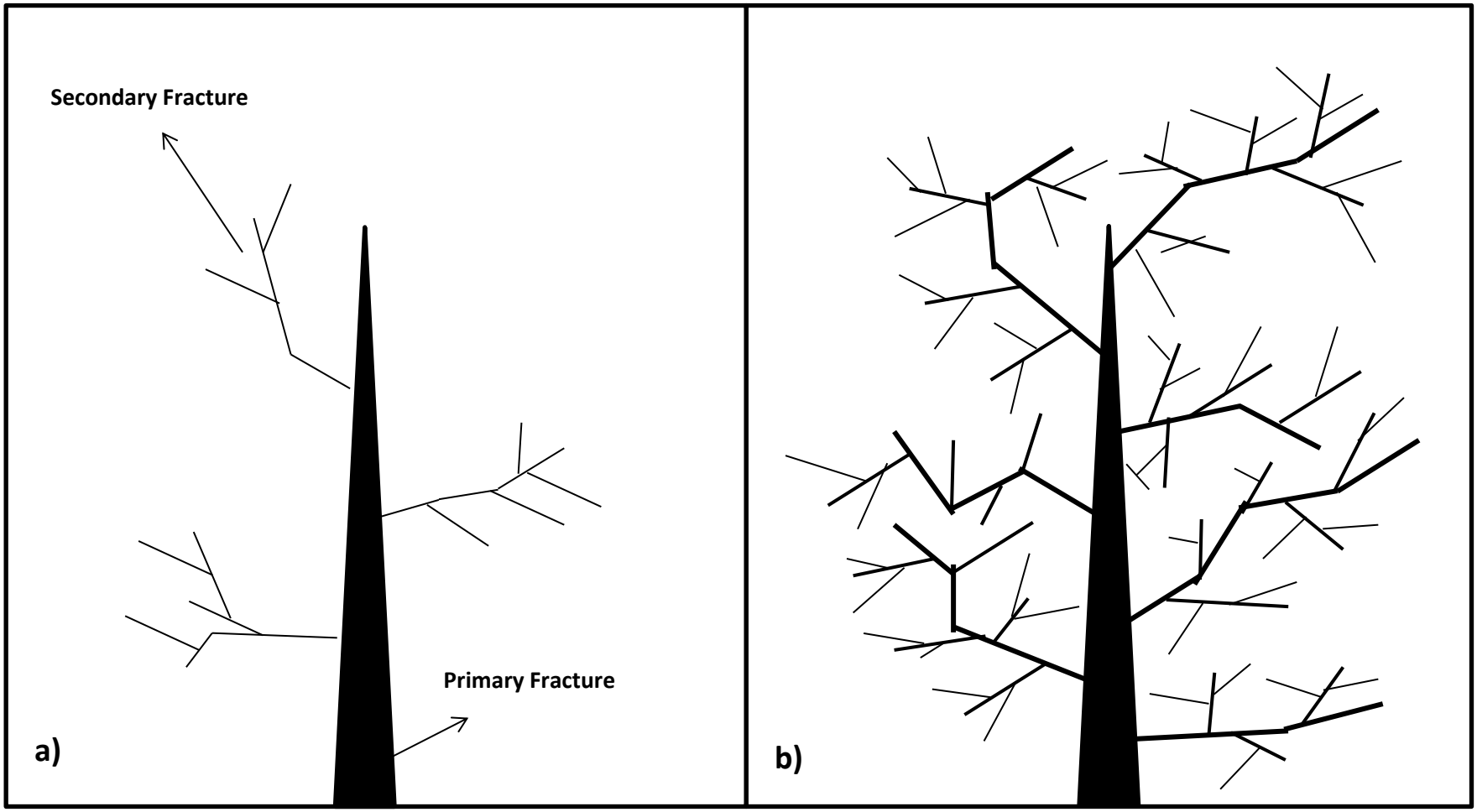

Figure2

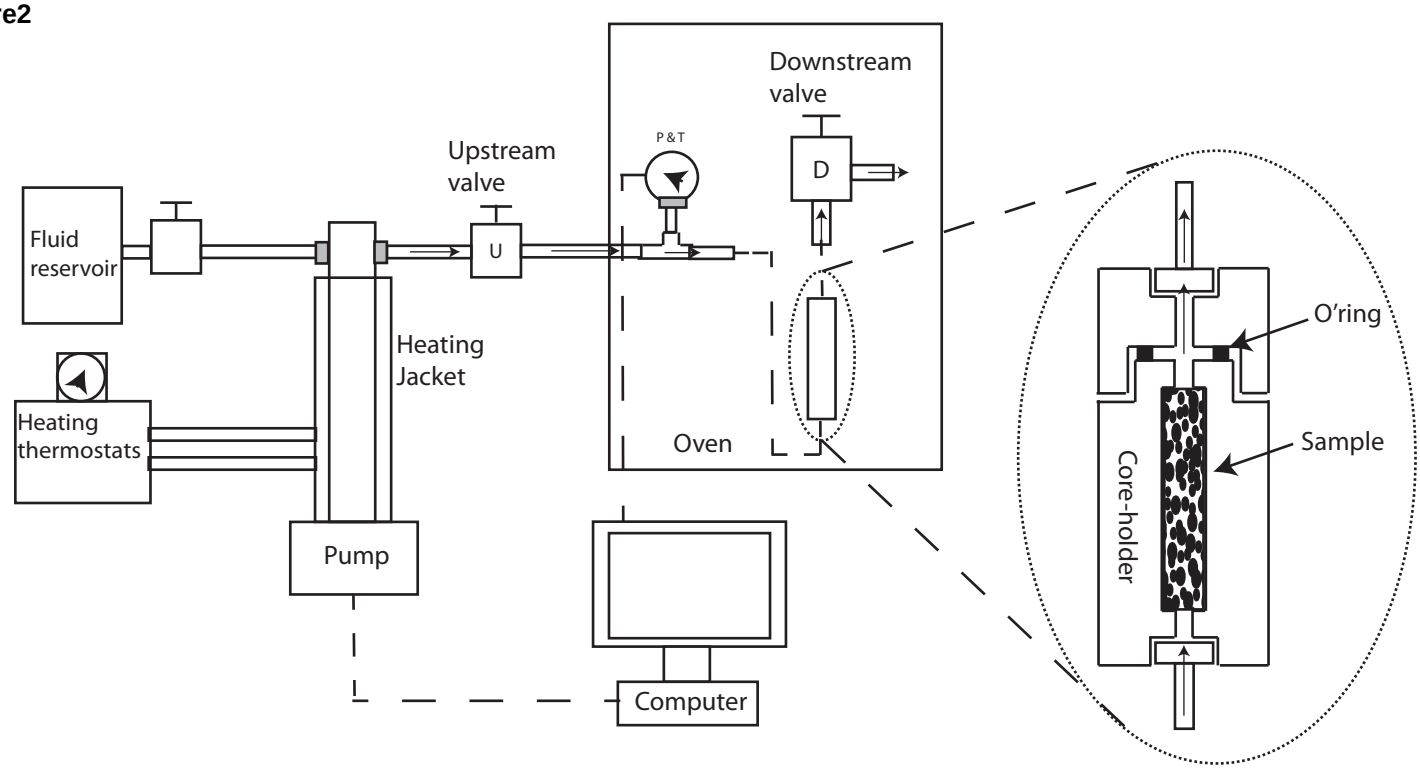
Downstream
valve
P&T
Upstream
valve
D
U
Fluid
reservoir
Heating
Jacket
Heating
thermostats
Oven
Pump
Computer
O'ring
Sample
Core-holder

Figure3

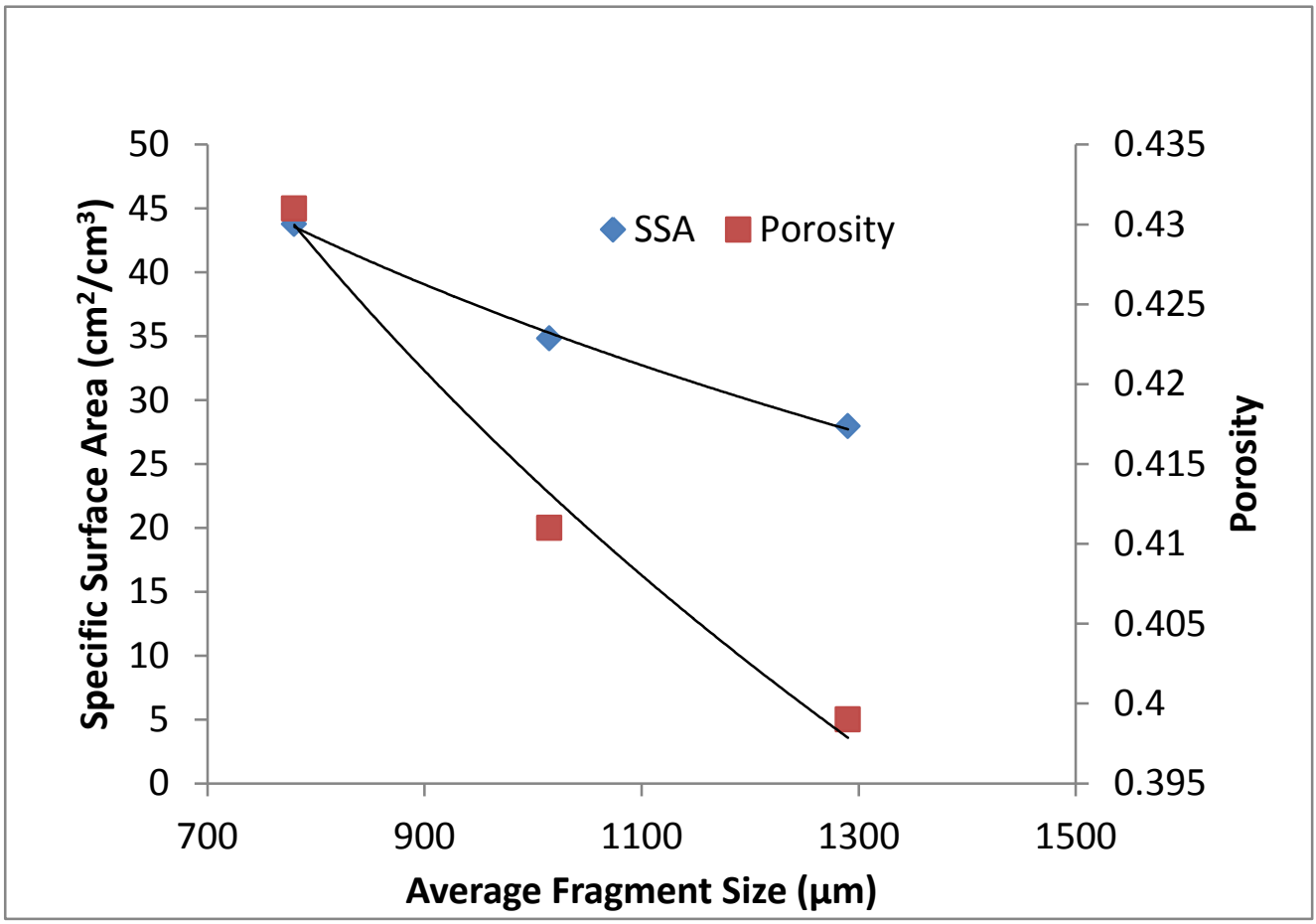
Specific Surface Area (cm²/cm³)
50
45
40
35
30
25
20
15
10
5
0
SSA
Porosity
0.435
0.43
0.425
0.42
0.415
0.41
0.405
0.4
0.395
Porosity
700
900
1100
1300
1500
Average Fragment Size (µm)

Figure4

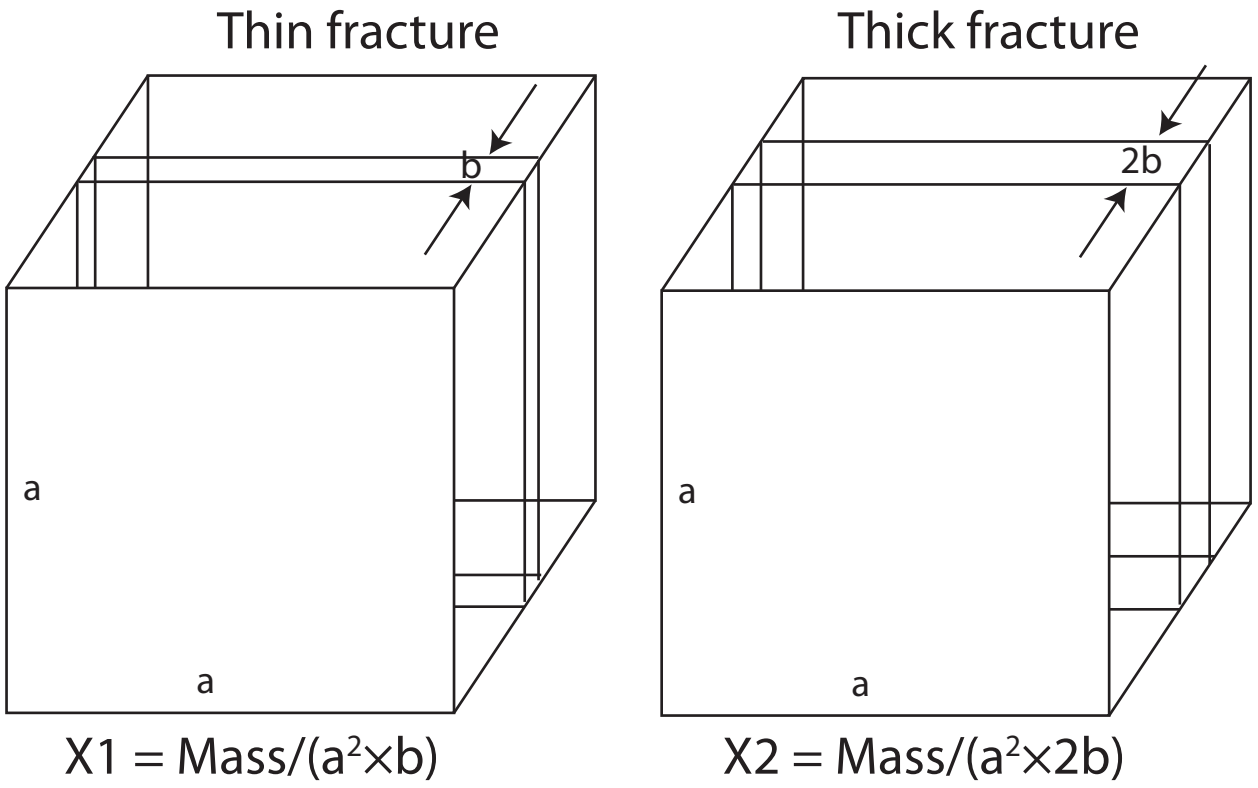
Thin fracture
Thick fracture
b
2b
a
a
a
a
X1 = Mass/(a²×b)
X2 = Mass/(a²×2b)

a)

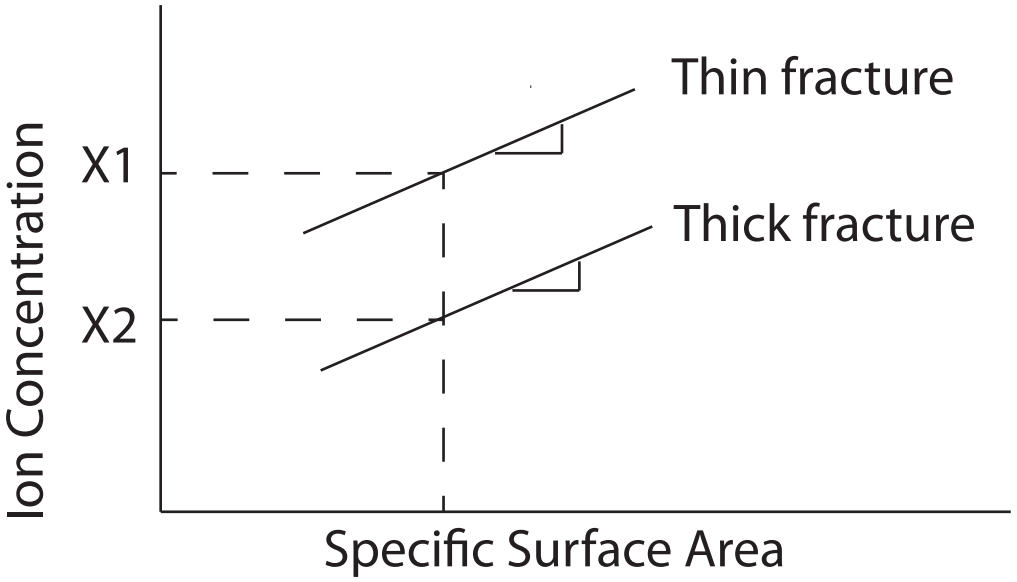
Thin fracture
Thick fracture
X1
X2
Ion Concentration
Specific Surface Area

b)

Figure5

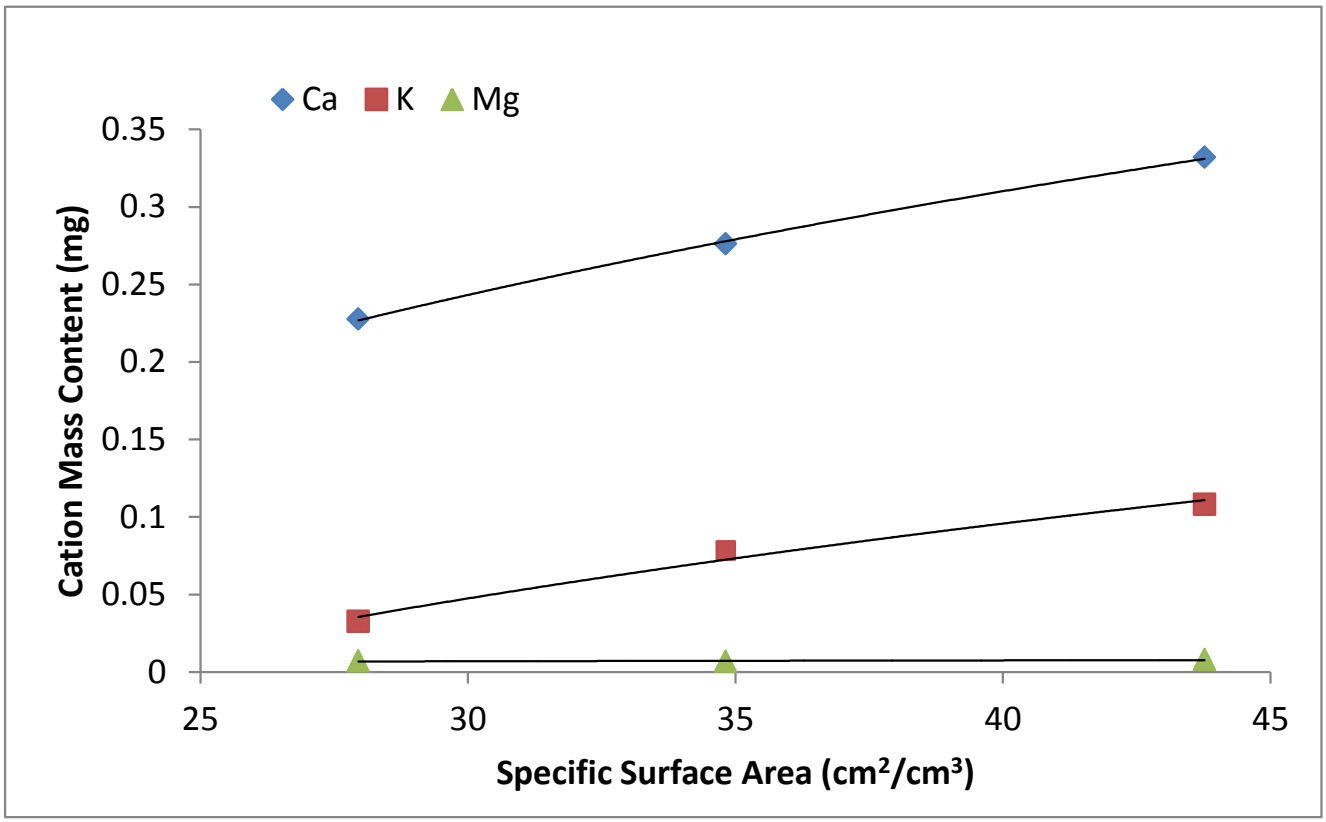
Ca
K
Mg
0.35
0.3
0.25
0.2
0.15
0.1
0.05
0
Cation Mass Content (mg)
25
30
35
40
45
Specific Surface Area (cm²/cm³)

Figure6

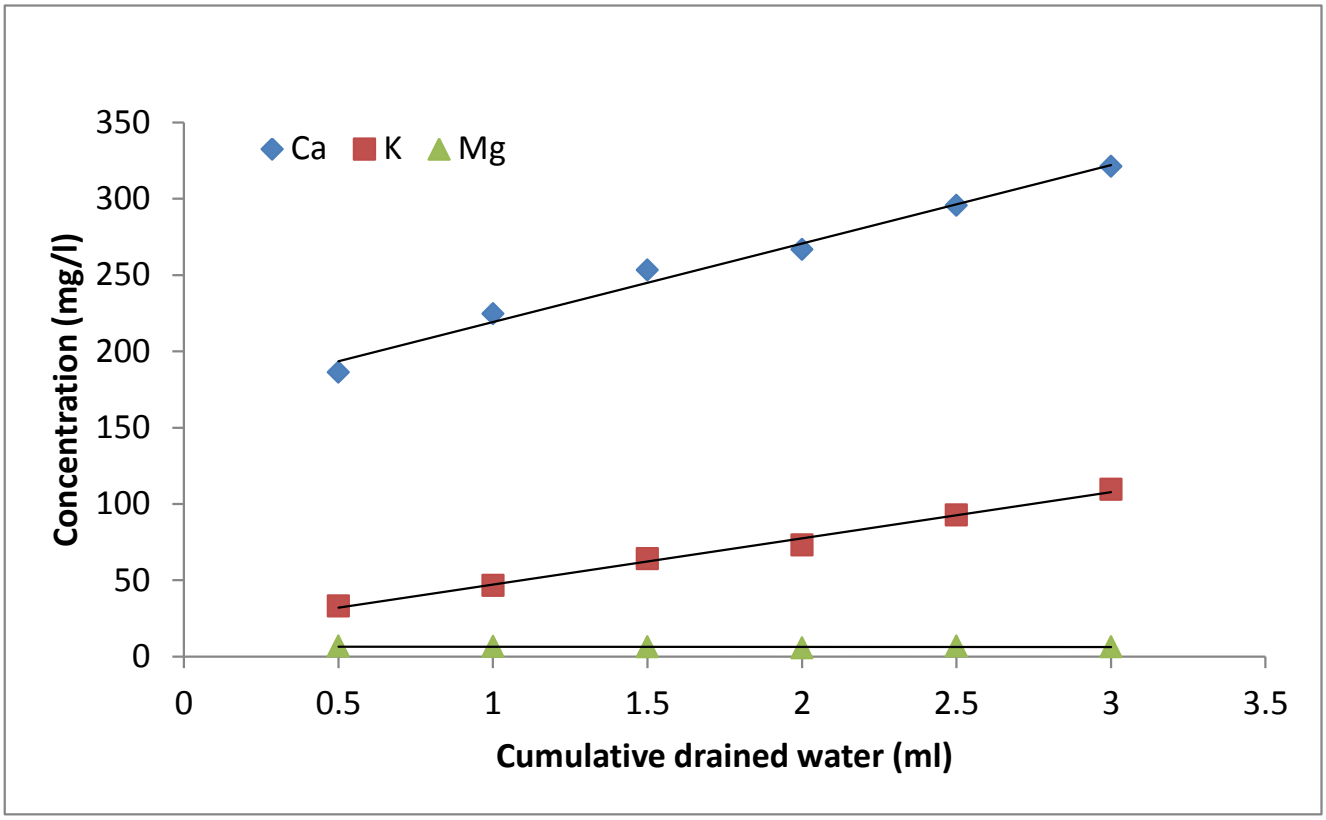
Ca
K
Mg
Concentration (mg/l)
350
300
250
200
150
100
50
0
0
0.5
1
1.5
2
2.5
3
3.5
Cumulative drained water (ml)

Figure7

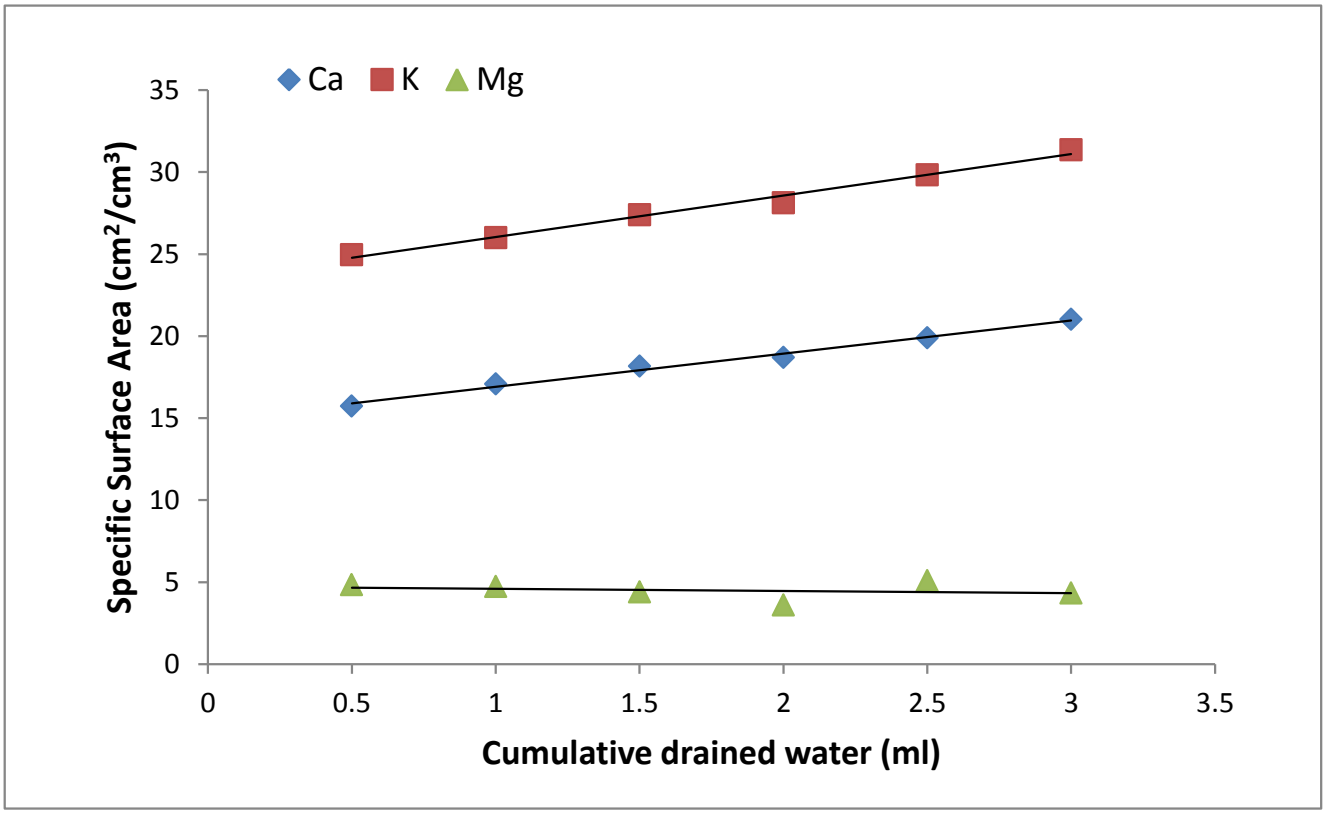
Ca
K
Mg
Specific Surface Area (cm²/cm³)
35
30
25
20
15
10
5
0
0
0.5
1
1.5
2
2.5
3
3.5
Cumulative drained water (ml)

Figure8

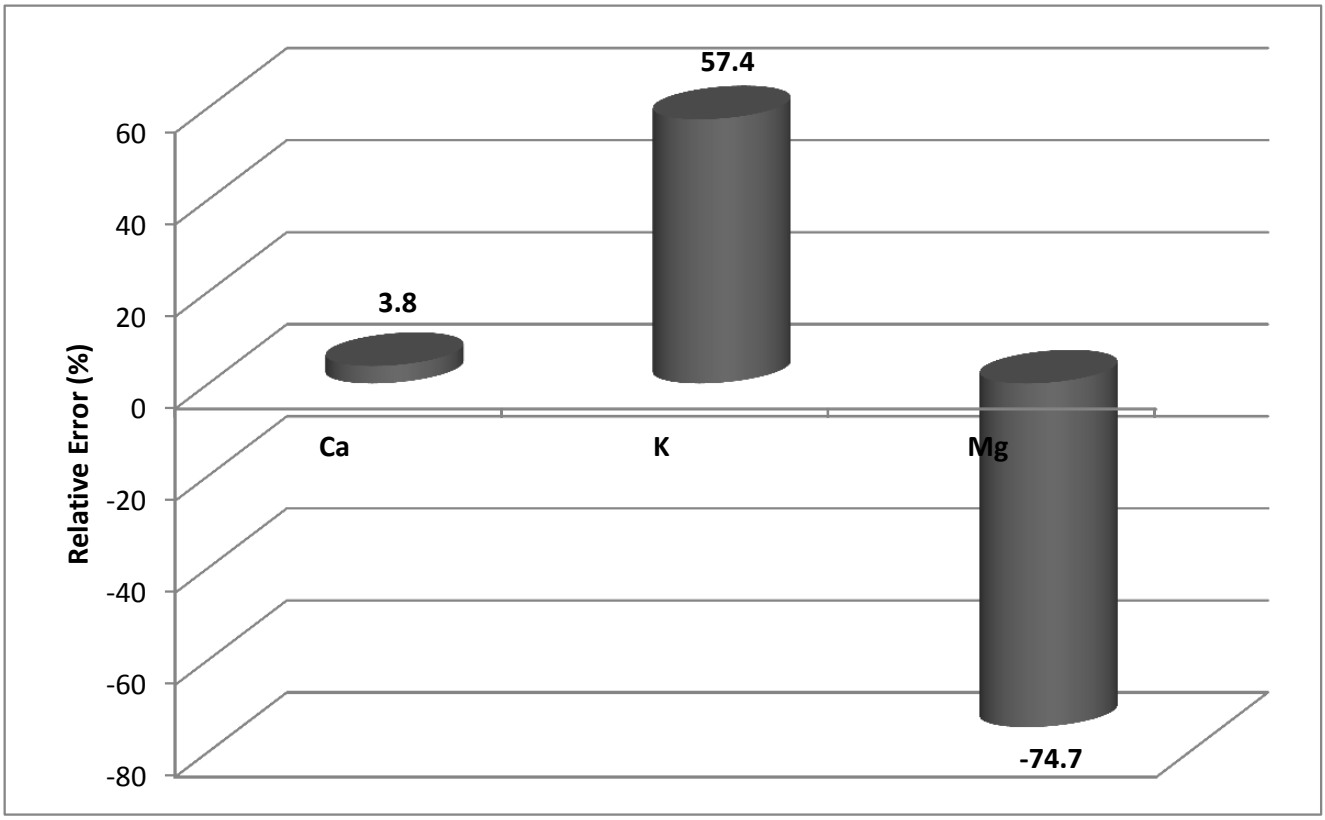

Table1

Click here to download Table: Table 1.docx

Cation	Ca	K	Mg	Na
Individual CEC (Meq/l)	6.89	1.9	0.1	-**

Table2

Click here to download Table: Table 2.docx

Ion	4 h (mg/l)	24 h (mg/l)	48 h (mg/l)
Ca^{2+}	0.46	0.47	0.41
K^{+}	4.4	4.45	4.6
Mg^{2+}	0.01	0.02	0.05